

**Pitch and Yaw Trajectory Measurement Comparison  
Between Automated Video Analysis and Onboard Sensor  
Data Analysis Techniques**

**by Ryan J. Decker, Bradford S. Davis, and Thomas E. Harkins**

ARL-TR-6576

September 2013

## **NOTICES**

### **Disclaimers**

The findings in this report are not to be construed as an official Department of the Army position unless so designated by other authorized documents.

Citation of manufacturer's or trade names does not constitute an official endorsement or approval of the use thereof.

Destroy this report when it is no longer needed. Do not return it to the originator.

# **Army Research Laboratory**

Aberdeen Proving Ground, MD 21005

---

**ARL-TR-6576**

**September 2013**

---

## **Pitch and Yaw Trajectory Measurement Comparison Between Automated Video Analysis and Onboard Sensor Data Analysis Techniques**

**Ryan J. Decker**

**Analysis and Evaluation Technology Division, ARDEC**

**Bradford S. Davis and Thomas E. Harkins**

**Weapons and Materials Research Directorate, ARL**

<b>REPORT DOCUMENTATION PAGE</b>			<i>Form Approved</i> <i>OMB No. 0704-0188</i>		
Public reporting burden for this collection of information is estimated to average 1 hour per response, including the time for reviewing instructions, searching existing data sources, gathering and maintaining the data needed, and completing and reviewing the collection information. Send comments regarding this burden estimate or any other aspect of this collection of information, including suggestions for reducing the burden, to Department of Defense, Washington Headquarters Services, Directorate for Information Operations and Reports (0704-0188), 1215 Jefferson Davis Highway, Suite 1204, Arlington, VA 22202-4302. Respondents should be aware that notwithstanding any other provision of law, no person shall be subject to any penalty for failing to comply with a collection of information if it does not display a currently valid OMB control number. <b>PLEASE DO NOT RETURN YOUR FORM TO THE ABOVE ADDRESS.</b>					
<b>1. REPORT DATE (DD-MM-YYYY)</b> September 2013		<b>2. REPORT TYPE</b> Final		<b>3. DATES COVERED (From - To)</b> September 2012–May 2013	
<b>4. TITLE AND SUBTITLE</b> Pitch and Yaw Trajectory Measurement Comparison between Automated Video Analysis and On-Board Sensor Data Analysis Techniques			<b>5a. CONTRACT NUMBER</b>		
			<b>5b. GRANT NUMBER</b>		
			<b>5c. PROGRAM ELEMENT NUMBER</b>		
<b>6. AUTHOR(S)</b> Ryan J. Decker*, Bradford S. Davis, and Thomas E. Harkins			<b>5d. PROJECT NUMBER</b> AH80		
			<b>5e. TASK NUMBER</b>		
			<b>5f. WORK UNIT NUMBER</b>		
<b>7. PERFORMING ORGANIZATION NAME(S) AND ADDRESS(ES)</b> U.S. Army Research Laboratory ATTN: RDRL-WML-E Aberdeen Proving Ground, MD 21005			<b>8. PERFORMING ORGANIZATION REPORT NUMBER</b>  ARL-TR-6576		
<b>9. SPONSORING/MONITORING AGENCY NAME(S) AND ADDRESS(ES)</b>			<b>10. SPONSOR/MONITOR'S ACRONYM(S)</b>		
			<b>11. SPONSOR/MONITOR'S REPORT NUMBER(S)</b>		
<b>12. DISTRIBUTION/AVAILABILITY STATEMENT</b> Approved for public release; distribution unlimited.					
<b>13. SUPPLEMENTARY NOTES</b> * Analysis and Evaluation Technology Division, U.S. Army Armament Research, Development and Engineering Center (ARDEC), Picatinny Arsenal, NJ					
<b>14. ABSTRACT</b> This report is a comparison between a newly developed method and a well proven analysis process to measure the pitch and yaw behavior of an artillery projectile following cannon launch. In the new method, launch video is processed using automated computer-vision algorithms to estimate a projectile's orientation history in the interval of video coverage. For the experiments covered by this report, this interval extended from the muzzle to approximately 70–80 m downrange. The accuracy of the method's results is validated by comparing them to results obtained from processing of high-fidelity onboard measurements using the vectoring technique known as Projectile Orientation In Navigation TERms (POINTER). From this evaluation, it is shown that the automated video analysis method is correctly measuring the epicyclic motion of the projectile during the portion of flight captured by the video (first two nutation cycles).  Included in the report is a general introduction of both analysis methods, as well as a brief overview of other techniques used by aeroballisticians to characterize the flight mechanics of artillery projectiles. The limits and advantages of the various methods are discussed, and future research efforts to improve results and overcome some of the shortcomings of the automated video method are identified.					
<b>15. SUBJECT TERMS</b> free-flight experimentation, pitch and yaw measurements, high-speed video, onboard instrumentation, telemetry					
<b>16. SECURITY CLASSIFICATION OF:</b>			<b>17. LIMITATION OF ABSTRACT</b>  UU	<b>18. NUMBER OF PAGES</b>  40	<b>19a. NAME OF RESPONSIBLE PERSON</b> Ryan J. Decker
<b>a. REPORT</b> Unclassified	<b>b. ABSTRACT</b> Unclassified	<b>c. THIS PAGE</b> Unclassified			<b>19b. TELEPHONE NUMBER (Include area code)</b> (973) 724-7789

---

## Contents

---

<b>List of Figures</b>	<b>iv</b>
<b>1. Introduction</b>	<b>1</b>
<b>2. New Experimental Ground-Based Method: Projectile Orientation Measured From Computer Vision Analysis of Launch Video</b>	<b>2</b>
<b>3. Previous Ground-Based Video Method Evaluation Results</b>	<b>6</b>
<b>4. Comparison Results From Experimental Data</b>	<b>7</b>
<b>5. Discussion of Benefits/Disadvantages of the Two Methods</b>	<b>13</b>
<b>6. Summary and Conclusions</b>	<b>14</b>
<b>7. References</b>	<b>16</b>
<b>Appendix A. The Aeroballistic Diagnostic Fuze (DFuze)</b>	<b>19</b>
<b>Appendix B. Projectile Orientation In Navigation TERms (POINTER)</b>	<b>23</b>
B-1 Solving for Projectile Heading - Generalized Solution.....	23
B-2 Solving for Projectile Heading - Application to Solar and Magnetic Sensor Data.....	24
B-3 Effect of Measurement Geometry on Accuracy of POINTER.....	28
<b>List of Symbols, Abbreviations, and Acronyms</b>	<b>33</b>
<b>Distribution List</b>	<b>34</b>

---

## List of Figures

---

Figure 1. Representative video frame from a flight experiment. ....	3
Figure 2. Automatic segmentation of the projectile shape and key-point identification. ....	4
Figure 3. Mapping video data to gun-fixed coordinate system. ....	5
Figure 4. Mapping data from camera frames to gun-fixed coordinate system. ....	5
Figure 5. Alpha-beta plot of initial projectile angular motion. ....	6
Figure 6. Equipment used during YPG flight experiments. ....	8
Figure 7. Estimated angle-of-attack components history, projectile no.1. ....	9
Figure 8. Comparison of angle-of-attack component estimates, projectile no.1. ....	10
Figure 9. Total angle-of-attack history comparison. ....	10
Figure 10. Alpha-beta history comparison, projectile no.1. ....	11
Figure 11. Estimated angle-of-attack components history, projectile no.2. ....	11
Figure 12. Comparison of angle-of-attack component estimates, projectile no.2. ....	12
Figure 13. Total angle-of-attack history comparison. ....	12
Figure 14. Alpha-beta history comparison, projectile no.2. ....	13
Figure A-1. Projectile state measurement systems. ....	20
Figure A-2. DFuze instrumentation on the front of an artillery round. ....	20
Figure B-1. A spinning body within a convenient navigation coordinate system. ....	24
Figure B-2. The “solar” coordinate system. ....	25
Figure B-3. Components of the projectile pointing vector in the “solar” system. ....	27
Figure B-4. Relative orientation of solar and magnetic vectors at experiment site. ....	29
Figure B-5. Angle between projectile heading and plane containing solar and magnetic vectors. ....	30
Figure B-6. POINTER suitability scoring at YPG experiment site. ....	31
Figure B-7. POINTER suitability scoring at YPG experiment site for two shotlines. ....	31
Figure B-8. POINTER suitability scoring at YPG experiment site for two test dates. ....	32
Figure B-9. POINTER suitability scoring at two experiment sites. ....	32

---

## 1. Introduction

---

Aeroballistic characterization is a critical step in the design and development of artillery projectiles. In whole or in part, these characterizations are often achieved during experimental flight testing wherein, “the main task is to determine from observations of a missile’s motion the values of the aerodynamic coefficients appearing in the differential equations describing that motion” (1). When measurements of the position, orientation, and velocity histories of projectiles in free-flight and descriptions of the associated ambient conditions are obtained, mathematical analyses yield estimates of the parameters needed to create six degree-of-freedom trajectory models of the subject projectiles. The fidelity of these models is directly related to the quantity and quality of observation measurements. These models serve as the basis for optimizing weapon performance, creating trajectory simulations, and are used to generate the firing tables that Soldiers will use to accurately aim their weapons.

There are several ways that ballistics engineers collect flight performance data. These methods are conveniently divided between those employing “observers” external to the projectiles (primarily ground-based) and those with “observers” on board the projectiles. Conventional ground-based methods long used to measure the projectile’s angular orientation history include yaw cards<sup>1</sup> (2) and spark ranges<sup>2</sup> (3), whereby the values of pitch and yaw at discrete locations from the muzzle of the weapon are determined by postflight analysis of the card perforations and shadowgraphs, respectively. Position and velocity information can also be derived from the times-of-arrival at the surveyed spark stations. These methods require extensive manual setup for each round fired, and limit the elevation angle of the cannon to near-horizontal firing conditions. In addition, these methods may not be suitable for projectiles that discard components like fin covers or sabots—or for some precision munitions that maneuver. Fixed-head and/or tracking radars are also routinely employed at test ranges to obtain velocity and/or position data.

The earliest description we have found of an experiment employing onboard systems to obtain estimates of free-flight projectile dynamics is that of Gotlieb et al. in 1948 (4). In this experiment, a projectile was equipped with a radio transmitter. The variations in signal strength at a ground receiving station were used to approximate the projectile’s yawing behavior. The Aeroballistic Diagnostic Fuze (DFuze) (5), patented<sup>3</sup> by the U.S. Army Research Laboratory (ARL) in 2002, includes multiple translational and angular motion sensors and a telemetry (TM)

---

<sup>1</sup>First employed by Fowler, et al., in 1920 as described in: R. Fowler, E. Gallop, C. Lock and H. Richmod, “The aerodynamics of a spinning shell,” *Philos. Trans. R. Soc. London, Ser. A*, **221**, pp. 295 (1921).

<sup>2</sup>The first spark range used for projectile aerodynamics determination was completed during World War II at the U.S. Army Ballistic Research Laboratory (BRL) at Aberdeen Proving Ground, MD. The earliest description and results are given in: W. Braun, A. Charters and R. Thomas, “Retardation of Fragments,” Report No. 425, U.S. Army Ballistic Research Laboratory, Aberdeen Proving Ground, MD, November 1943.

<sup>3</sup>U.S. Patent #6349642, Hepner, et al., *Aeroballistic diagnostic system*, February 2002.

system to continuously collect and broadcast data from prelaunch to impact. These data are recorded and postprocessed to estimate both in-bore and in-flight projectile dynamics histories. Using an ARL-patented vector matching technique<sup>4</sup> termed POINTER—Projectile Orientation In Navigation TERms—projectile attitude histories are derived from DFuze optical and magnetic sensor data. Particularly since the onset of the microelectronics revolution, the variety and number of sensing and communications devices available for use onboard gun- and tube-launched projectiles is continually expanding, thereby providing the test and evaluation community with increasing instrumentation options. This report describes a new ground-based method to obtain state measurements using multiple external video cameras that is under development by the U.S. Armaments Research and Development Center (ARDEC) and the Naval Postgraduate School (NPS). Once the video data are acquired, this method is fully automated and can provide near launcher muzzle projectile attitude measurements within minutes. Not only does this represent a new source of projectile data useful for postexperiment aerodynamic characterization, but the potential availability of near real-time launch dynamics data can enable decisions during the execution of flight experiments that significantly contribute to achieving test goals in an efficient and economic manner.

In the next three sections of this report, the method will be summarized and examples provided of angular measurements that were obtained with this video technique (section 2); results from comparison of angular measurements made for computer-generated (i.e., perfect) synthetic projectile video and from comparison of measurements made during flight experiments at a single downrange location will be discussed (section 3); and comparisons of video-derived angular measurements will be made to those obtained with the onboard POINTER method from several flight experiments (section 4).

Some of the advantages and limitations of these two methods will be discussed in section 5. Expected and recommended future efforts will be listed in the final section. Details of the DFuze system and the POINTER methodology are given in appendices A and B.

---

## **2. New Experimental Ground-Based Method: Projectile Orientation Measured From Computer Vision Analysis of Launch Video**

---

At many artillery flight experiments, sophisticated optical instruments—such as the Trajectory Tracker (6) or Flight Follower (7) systems—are used to capture video of a cannon launch and the initial part of a projectile free-flight. These systems use rotating mirrors to keep the round in view, while recording the images with ultra high-speed cameras. The experimental method being

---

<sup>4</sup>U.S. Patent # 6398155, Hepner and Harkins, *Method and system for determining the pointing direction of a body in flight*, June 2002.

evaluated in this report uses the video captured by these systems to estimate the orientation history of the projectile. For convenience, hereafter we will call this the “video method.”

The automated video method begins by collecting important information from the header that is a part of each video frame. Included in the header is the test range standard International Range Instrumentation Group (IRIG) time (8) when the frame was recorded. This time base is used with all test range instrumentation (radars, TM recorders, etc.) to establish time correspondence of data acquired from independent systems. Figure 1 shows an example of a video frame and some of the information that is extracted with optical character recognition software. In addition, the orientation angle history of the camera system as the mirror rotates is automatically read into the analysis.

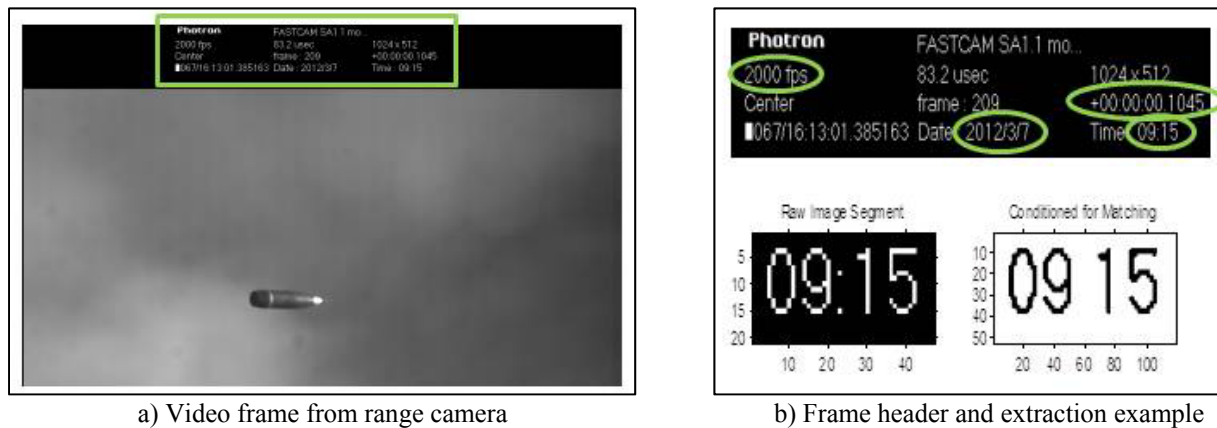


Figure 1. Representative video frame from a flight experiment.

Using a sequence of morphological operations and computer-vision algorithms, the shape of the projectile is identified in each frame of the video as illustrated in figure 2. With subpixel accuracy, the central moment and nose location are determined (indicated by the large and small red plus signs, respectively). From the relative position of these two points, the apparent pitch angle of the projectile in the frame is measured. Corrections to the pitch angle history are then made to account for the perspective skew angle and any deviation between the projectile’s velocity vector angle and the horizontal axis of the video frame. Details of this correction methodology are reported separately (9).

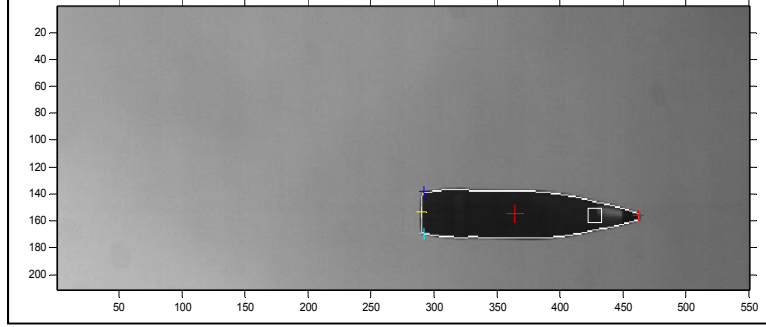


Figure 2. Automatic segmentation of the projectile shape and key-point identification.

When two distinct video systems provide simultaneous imagery from different perspectives, the resolved orientation history of the projectile during the initial phase of free-flight can be estimated in any desired coordinate system. With a priori knowledge of the cannon and camera locations and the camera orientation angles for each frame, the video data can be mapped into the gun-fixed coordinate system, in which trajectories most often are described per the geometry illustrated in figure 3. The projectile's location (downrange, crossrange, altitude) and heading (elevation -  $\vec{P}_\theta$ , azimuth -  $\vec{P}_\psi$ ) during the initial trajectory are thus estimated, see figure 4. When these heading vector components are differenced from the corresponding elevation and azimuth components of the projectile's velocity vector ( $\vec{V}_\theta, \vec{V}_\psi$ ) and corrected for the azimuth plane foreshortening, the pitch plane and yaw plane components ( $\vec{P}_\alpha, \vec{P}_\beta$ ) of the projectile angle-of-attack remain, i.e.,

$$(\vec{P}_\alpha, \vec{P}_\beta) = \left( \vec{V}_\theta - \vec{P}_\theta, \left[ \frac{\vec{V}_\psi - \vec{P}_\psi}{\cos \vec{P}_\theta} \right] \right) . \quad (1)$$

If these components are graphed versus each other, the well known alpha-beta plot of projectile angular motion is produced, see figure 5. When at the range conducting free-flight experiments, once video camera data are loaded, these critical initial angular motion histories can be provided to test engineers at the gun site within minutes of the projectile being fired.

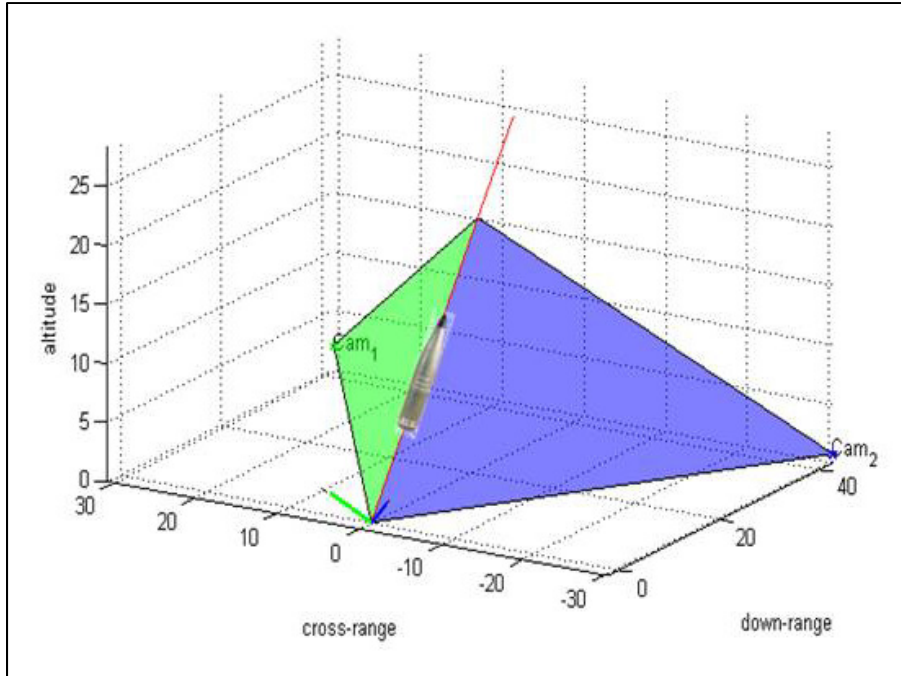


Figure 3. Mapping video data to gun-fixed coordinate system.

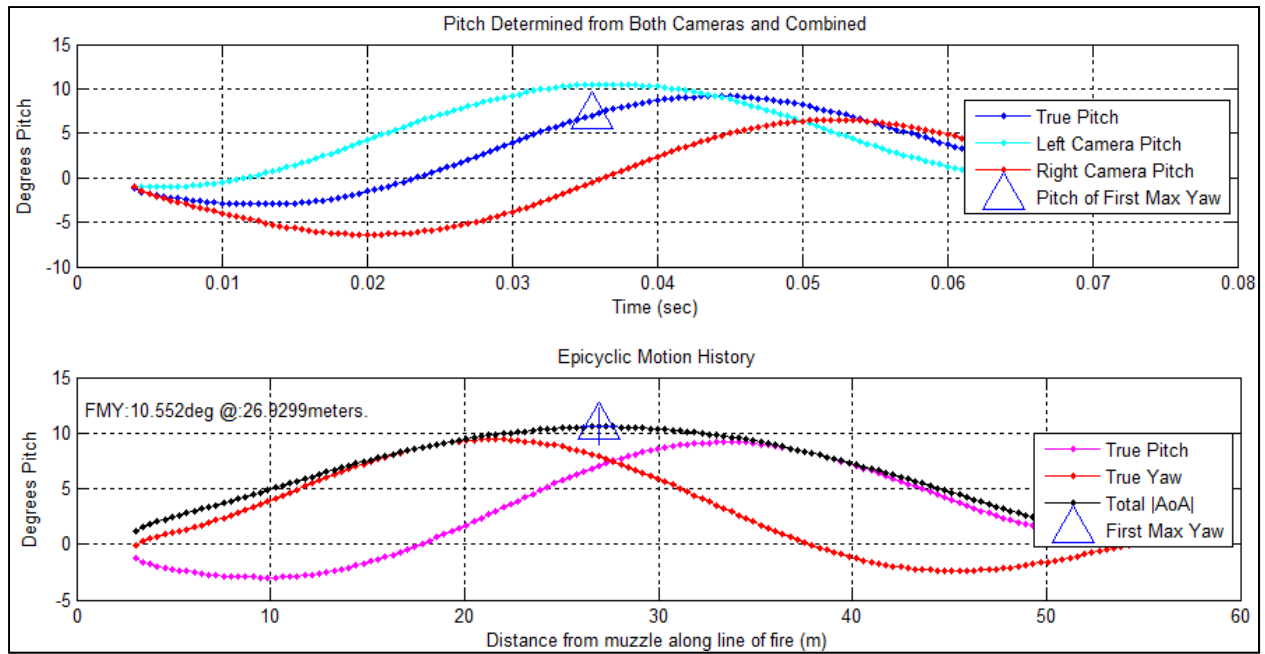


Figure 4. Mapping data from camera frames to gun-fixed coordinate system.

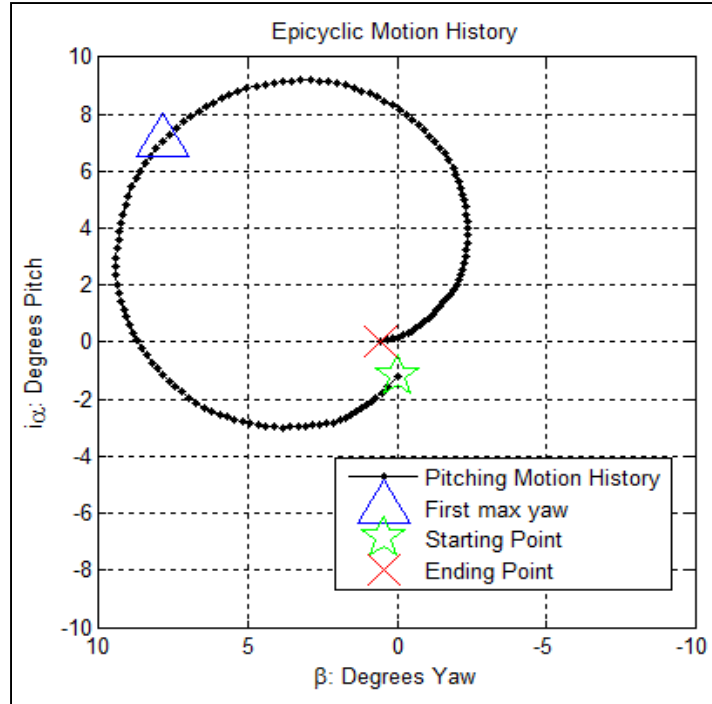


Figure 5. Alpha-beta plot of initial projectile angular motion.

---

### 3. Previous Ground-Based Video Method Evaluation Results

---

Previously, the automated video method was exercised using synthetic launch videos generated from computer-aided design software. These videos were designed to match anticipated test-range video in resolution, signal duration, and ambient light intensity. When the synthetic videos were analyzed, the measured pitch angle was accurate to within a small fraction of a degree for each frame (9). These results validated the projectile shape extraction procedure and the mathematical formulation of the mapping operations of the video method. However, when using the automated video method with actual test-range video, there are potential sources of error affecting the video frame image quality that were not present in the synthetic videos. Individual lens aberrations may distort the image in each captured frame. The projectile may be partially or wholly concealed in near muzzle images by blow-by smoke and other obscurants resulting from the gun blast. The instantaneous relative locations of the projectile, the camera, and the sun may result in glint on the projectile surface and/or glare that compromise the image. Random noise from the video-capture process and potential camera shaking from the launch shockwave can degrade image quality. Additionally, the projectile naturally comes slightly into and out of focus because the line of sight range rapidly changes as the projectile progresses along its trajectory. Finally, it is not unusual for there to be some number of frame dropouts in field experiment data.

Using real launch videos collected during flight experiments conducted in September 2012, the accuracy of the video method at a single downrange location was examined. In this effort, the video-method-derived estimates of pitch and yaw at a position of approximately 25 m from the cannon were compared to values derived by manual analysis from photographs taken by two fixed-perspective cameras located underneath and perpendicular to the anticipated trajectory at that location, respectively. The comparison from more than 800 rounds yielded an average difference between the automated video-method-derived projectile angle-of-attack magnitude and the manual fixed-perspective-derived angle-of-attack magnitude of  $0.25^\circ$ , with a standard deviation of  $1.30^\circ$  (10). These results constitute a qualitative rather than a quantitative assessment because the accuracy of the manual analysis is not known and the fixed-perspective cameras locations and orientations were not precisely surveyed as they would have been in a spark range.<sup>5</sup>

Encouraged by these results at a single data point for each shot, it was decided to compare pitch and yaw history estimates from the automated video method to pitch and yaw history estimates from POINTER analysis of DFuze data.

---

#### **4. Comparison Results From Experimental Data**

---

In October 2012, a flight experiment was conducted at Yuma Proving Grounds (YPG), AZ. on a developmental 155-mm artillery projectile for aerodynamic characterization purposes. Included in this experiment were 10 projectiles equipped with TM instrumentation packages. As is common in flight experiments undertaken to collect projectile dynamics data for aerodynamic characterization, the cannon was fitted with a half-muzzle brake, which creates a region near the muzzle with asymmetric applied loads on the projectile (12). This is done to impart enough angular motion for accurate determination of all aerodynamic coefficients and derivatives of interest (13, 14). At the same time, the resulting larger amplitude angles-of-attack at muzzle exit provided better opportunities for comparison of results from the video method and POINTER processing than might otherwise have occurred. Pictures of some of the experimental hardware can be seen in figure 6.

---

<sup>5</sup>It is believed that the accuracy of the manual reduction method is on the order of  $1^\circ$  as that is the level of accuracy of angular measurements obtained from yaw-card analysis, which suffers from similar limitations. See McCoy (11) p 319.



a) M109 Cannon



b) Half-muzzle brake



c) Trajectory tracker



d) DFuze installed on an experiment projectile

Figure 6. Equipment used during YPG flight experiments.

Of the 10 rounds, only 6 were equipped with DFuzes that included both the optical and magnetic sensors whose output are necessary for POINTER processing. For two of these launches, the relative orientations of the solar vector, the geofield vector, and the projectile velocity vector were ill-suited for achieving accurate projectile-orientation measurements via POINTER (see appendix B). At the same time, there were also problems with the collection of video data for some of the flights. In two instances, the mirror did not move at the correct velocity, causing the bullet to leave the viewable window. In another launch, the sun was directly in the field-of-view of one of the cameras, causing much of the flight to be washed out. In two other launches, despite the half-muzzle brake, there was not enough yawing motion of the projectile for a valid measurement. Consequently, there only were two rounds with appreciable yawing motion where both the DFuze results and the automated video results were of sufficient quality to warrant comparison.

In similar future experiments, care should be taken to avoid test-range geometries that degrade the quality of the video and/or DFuze data. Whenever practicable, this can be done by making judicious choices of test location, time of day, and/or azimuth of fire (see appendix B).

Figure 7 gives the early postlaunch angle-of-attack history estimated via both POINTER and the video method for the first of the experimental rounds. In both cases the elevation and azimuth components of the projectile heading vector are estimated on a point-by-point basis whenever the respective optical/magnetic and image data are available. Output of magnetic sensors typically give angular estimates at rates of tens of kilohertz, but optical sensor-data processing yields angular estimates at a rate given by the product of the instantaneous projectile roll rate and the number of optical sensors around the projectile perimeter. In this case, the launch spin was approximately 226 Hz and there were four optical sensors. Hence, the POINTER rate at launch was 904 estimates/second (s). The frequency of video method estimates is the frames/s rate of the video cameras. For this experiment that rate was 2000 frames/s. After the heading vector, estimates are generated by each method; they are differenced from the corresponding velocity vector estimates to yield the angle-of-attack components in elevation and azimuth. A single Euler rotation then yields the alpha and beta components of the angle-of-attack.

The estimates of the alpha and beta angles for experiment projectile no. 1 during its first second of flight are seen in figures 7a and b, respectively. Muzzle exit time (time zero) was estimated using an infrared detector slaved to the tracking radar. The video method estimates are limited to the interval of camera coverage, which ended after approximately 120 ms of flight time; whereas, POINTER processing potentially can provide heading estimates throughout an entire trajectory. The POINTER estimates show the projectile is exhibiting the two mode (i.e., precession and nutation) epicyclic yawing motion that is typical of spinning symmetric bodies. The precession motion is seen to have a period of approximately 0.4 s (2.5 Hz). The video method estimates also evidence the existence of two mode yawing motion but they did not cover a long enough interval to characterize the precessional motion. Two periods of the initial nutation motion were captured by the video method with durations of approximately 0.057 s (17.5 Hz).

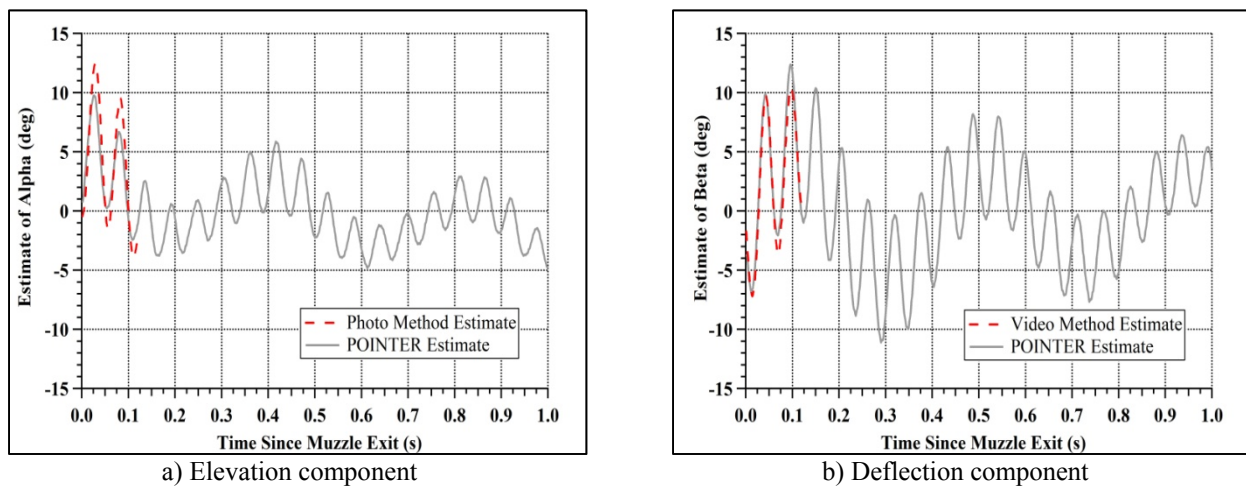


Figure 7. Estimated angle-of-attack components history, projectile no.1.

Zooming in on the interval covered by both methods (figure 8), agreement between the two methods is seen to be excellent in frequency, although there is some difference in the amplitude of the respective alpha estimates.

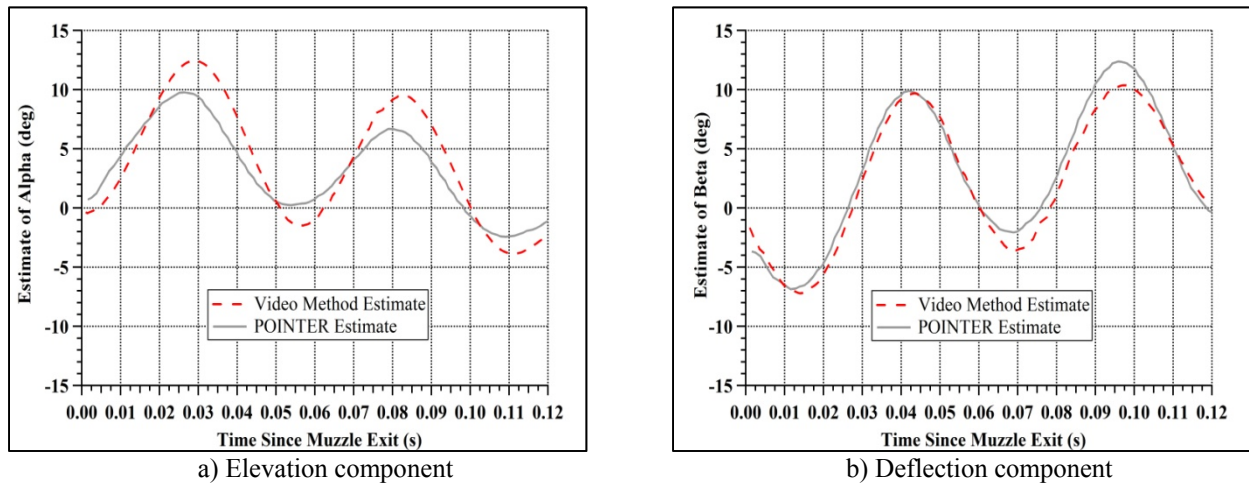


Figure 8. Comparison of angle-of-attack component estimates, projectile no.1.

The total angle-of-attack estimates are shown in figure 9. The truncation of the peak of the first hump in the POINTER estimate suggests that there is some inaccuracy in the POINTER estimates in that region, as the expected shape of such curves at projectile launch is like that of a rectified sine wave. Similar anomalous regions occur in the intervals of 150–225 ms, 400–450 ms, 600–650 ms, and 850–875 ms. Fitting of these data with rectified sine waves is sometimes done to smooth the estimates.

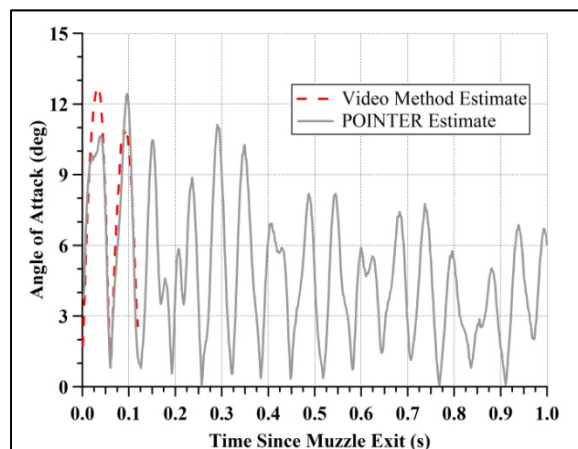


Figure 9. Total angle-of-attack history comparison.

Figure 10 shows the alpha-beta estimates from the two methods during the initial 120 ms of flight.

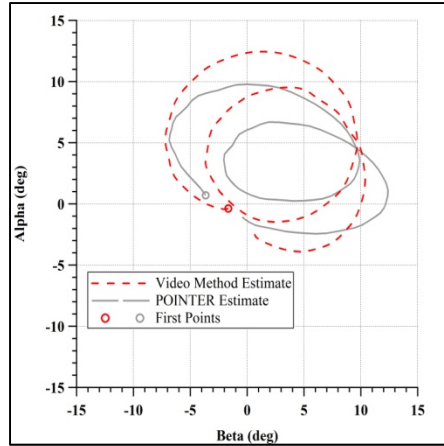


Figure 10. Alpha-beta history comparison, projectile no.1.

The estimates of the alpha and beta angles for experiment projectile no.2 during its first second of flight are seen in figures 11a and b, respectively. The camera coverage for this experiment yielded video method estimates for approximately 103 ms of flight time. The precession motion had a period of approximately 0.54 s (1.9 Hz frequency). As before, the video method estimates also evidence the existence of two mode yawing motion but they did not cover a long enough interval to characterize the precessional motion. One and one-half periods of the initial nutation motion were captured by the video method, with durations of approximately 0.064 s (15.6 Hz frequency). The ratios of these precession and nutation frequencies to those estimated for projectile no.1 agree well with the ratios of the respective launch velocities and spin rates.

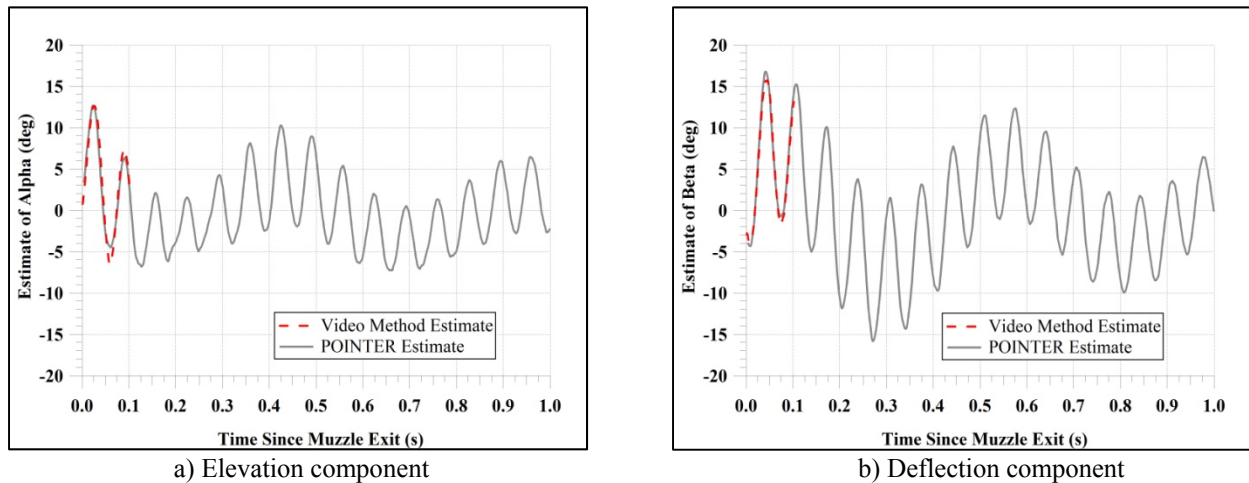
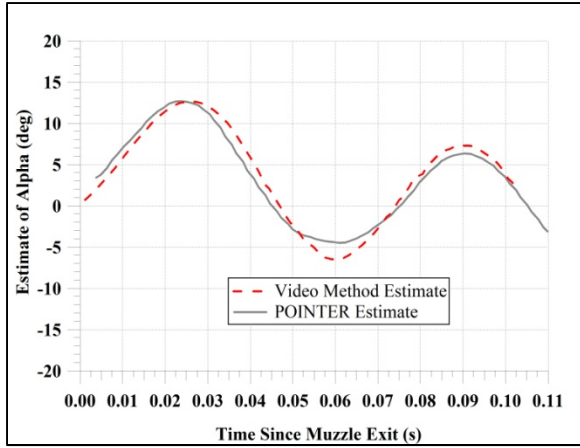
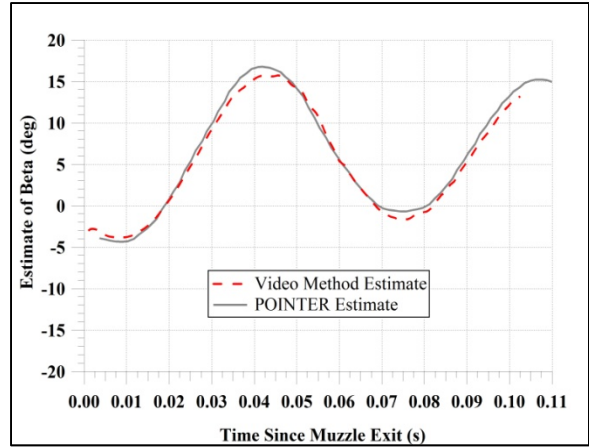


Figure 11. Estimated angle-of-attack components history, projectile no.2.

Zooming in on the interval covered by both methods (figure 12), agreement between the two methods is seen to be excellent in frequency and amplitude for both components.



a) Elevation component



b) Deflection component

Figure 12. Comparison of angle-of-attack component estimates, projectile no.2.

The total angle-of-attack estimates are shown in figure 13 and the alpha-beta estimates during the initial 103 ms of flight are shown in figure 14. Excellent agreement is seen in both instances.

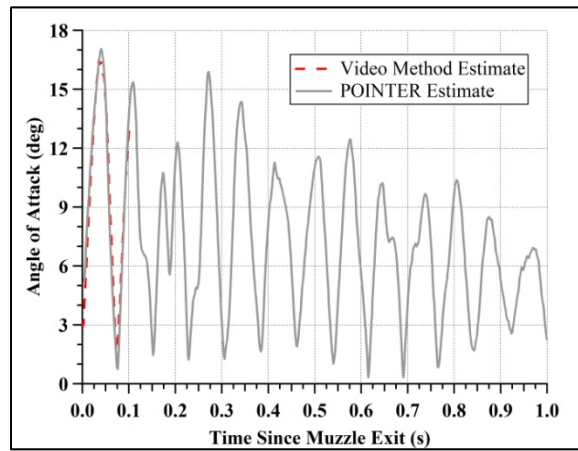


Figure 13. Total angle-of-attack history comparison.

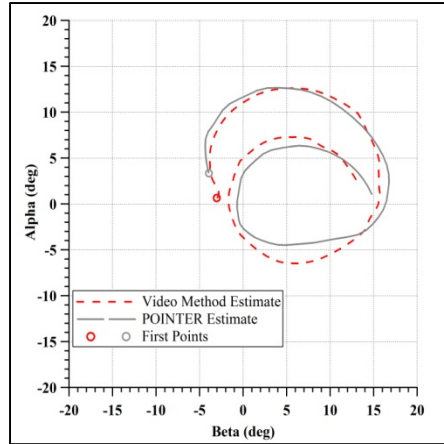


Figure 14. Alpha-beta history comparison, projectile no.2.

---

## 5. Discussion of Benefits/Disadvantages of the Two Methods

---

A significant limitation of the automated video analysis method is that there is a tradeoff between the amount of flight captured and the resolution of the projectile in the video frame from each camera. In the configuration tested in this report, the camera systems were positioned 40 m from the azimuthal line-of-fire. As was seen in the angular estimates, this allowed the capture of approximately 2 nutation cycles, but not enough data to characterize a complete precession cycle. The short length of flight captured is suitable for measuring initial angular momentum but longer intervals of videos are needed for aeroballistic characterization. If the cameras were positioned 133 m off of the azimuth of fire at a distance of 150 m downrange, a full precessional period would be covered by the camera field-of-view. Unfortunately, at this increased distance the resolution of the camera systems used for these experiments is such that the number of pixels covering the projectile would be reduced to a point that they would be insufficient for an accurate segmentation and measurement of the pitch angle. This shortcoming could be addressed either with higher resolution video from increased standoff distances, or with more cameras having the current resolution but positioned further downrange to provide additional intervals of coverage. With such longer duration observations, estimation of additional aerodynamic coefficients (e.g., drag) might be achieved. This possibility may be limited somewhat for elevated quadrant elevation (QE) shots due to rapidly increasing projectile altitude.

Aeroballistic experimentation and onboard instrumentation analysis is expensive. The video systems and the technician labor required to operate them are costly as well. However, many test plans already call for video systems to be used for other purposes. Therefore, the automated video analysis method is able to leverage a cost that may already be in place.

As the video and POINTER methods are mathematically similar, they are subject to similar geometric constraints affecting the precision of their angular measurements. For the video analysis method, it is ideal to have two orthogonal views of a projectile whose velocity vector is collinear with the intersection of the two image planes. Likewise, in the ideal geometry for POINTER, the vector from the projectile to the sun, the local geofield vector, and the projectile velocity vector form an orthogonal triad. Clearly, it is not physically possible to achieve this ideal. For the video method, it is notionally easy to place two cameras under and perpendicular to the shotline at some downrange distance, but the three pairwise included angles between the velocity vector and the vectors from the projectile to the two cameras are constantly changing as the projectile moves downrange. For POINTER, there are little or no changes in relative orientations of the solar, magnetic, and velocity vectors in early flight but it is seldom possible to achieve the ideal launch geometry. For projectiles in ballistic flight, the inertial heading of the velocity vector obviously changes as the projectile continues on its trajectory. Ergo, the included angles between the velocity vector and the sun and geofield are also changing. Additional concerns for the video method are image washout if a camera is looking into the sun and/or glint from the projectile degrading image quality. All of these geometric concerns can and should be addressed during experiment planning. As the geofield vector changes with location, altitude, and date; the solar vector changes with location, date, and time of day; and the gun shotline can change with test site; available options can be analyzed to design a test plan that achieves the best possible measurement conditions (see appendix B-3).

Several planned enhancements to the video analysis method are nearing completion. An automatic lens calibration algorithm is being implemented to counter the effects of lens aberrations. Also, an automated spin-rate computation algorithm has been developed and demonstrated using period measurements between successive sightings of longitudinal stripes painted on the ogive regions of experiment projectiles (15, 16). These measurements can be made using any identifiable fiducial mark on the projectile surface that can be extracted from the video.

In future field experiments, the cameras will be placed farther downrange to capture a longer portion of free-flight. Finally, we hope to employ additional pairs of video systems located even farther downrange to enable measurement of the complete precession cycle and evaluate drag coefficient estimation.

---

## 6. Summary and Conclusions

---

A new method to estimate projectile angular measurements near the launcher muzzle has been developed and demonstrated by ARDEC and NPS. In this method, images obtained from multiple ground-based tracking video camera films of projectiles early in flight are automatically processed using computerized algorithms to obtain an angular orientation history. Measurements

made with this system compared favorably with static measurements and angular histories obtained with the ARL TM-based DFuze/POINTER system. With this video method, initial projectile heading and angular rate can be obtained within minutes after the video record is obtained. Such a near real-time measurement capability could greatly impact field experiment economy and efficiency by providing critical feedback during testing.

The primary limitation of this method is the small amount of in-flight coverage available from a typical two-camera range instrumentation configuration. With greater coverage, additional aeroballistic measurements might be enabled. Options for achieving this are being investigated.

---

## 7. References

---

1. Whyte, R.; Jeung, A.; Bradley, J. *Chapman-Kirk Reduction of Free-Flight Range Data to Obtain Aerodynamic Coefficients*; BRL-MR-2298; U.S. Army Ballistic Research Laboratory: Aberdeen Proving Ground, MD, May 1973.
2. Arrow Tech Associates, Inc., “Use of Yaw Cards During Projectile Development,” Yaw Card White Paper, July 2010.
3. Davis, B.; Guidos, B.; Harkins, T. *Complementary Roles of Spark Range and Onboard Free-Flight Measurements for Projectile Development*; ARL-TR-4910; U.S. Army Research Laboratory: Aberdeen Proving Ground, MD, August 2009.
4. Gotlieb, C.; Pashler, P.; Rubinoff, M. A Radio Method of Studying the Yaw of Shells. *Can. J. Res., A* **May 1948**, *26*, 167–198.
5. Davis, B.; Harkins, T.; Patton, B.; Hall, R. *Aeroballistic Diagnostic Fuze (DFuze) Measurements for Projectile Development, Test, and Evaluation*; ARL-TR-3204; U.S. Army Research Laboratory: Aberdeen Proving Ground, MD, July 2004.
6. Specialised Imaging. *Trajectory Tracker User Manual*. 41690 Enterprise Circle North. Temecula, CA, 92590.
7. Itronix. “DRS’s Flight Follower System.” Specification Sheet. [www.itronix.com/pdf/DRS\\_Flight\\_Follower.pdf](http://www.itronix.com/pdf/DRS_Flight_Follower.pdf). (Accessed July, 2012).
8. IRIG STANDARD 200-04. Timing Committee, Telecommunications and Timing Group, Range Commanders Council. U.S. Army White Sands Missile Range, NM, September 2004.
9. Decker, R.; Kolsch, M.; Yakimenko, O. An Automated Method for Computer Vision Analysis of Cannon-Launched Artillery Video. *Proceedings of the 27th International Ballistics Symposium*, Freiburg, Germany, 2013.
10. Decker, R.; Kolsch, M.; Yakimenko, O. *Artillery Pitch and Yaw Measurement Test Report: An Automated Video Analysis Method to Measure First Maximum Yaw*; Naval Postgraduate School, Monterey, CA, report in preparation.
11. McCoy, R. *Modern Exterior Ballistics: The Launch and Flight Dynamics of Symmetric Projectiles*; Schiffer Publishing: Atglen, PA, 1999.
12. Davis, B.; Guidos, B. A Synopsis of Yaw-Induction Techniques used during Projectile Free-Flight Aerodynamics Experiments. *63rd Aeroballistic Range Association Meeting*, Brussels, Belgium, October 2012.

13. Davis, B.; Hathaway, H.; Hathaway, A.; Thompson, A. *Extending Telemetry Reduction to Aerodynamic Coefficients and Trajectory Reconstruction (EXTRACTR) Flight Experiment Using 155-mm M483A1 Projectiles*; ARL-TR-3563; U.S. Army Research Laboratory: Aberdeen Proving Ground, MD, August 2005.
14. Topper, B.; Brown, T.; Bukowski, E.; Davis, B.; Hall, R.; Muller, P.; Vong, T.; Brandon, F. *Feasibility of Determining Aerodynamic Coefficients for a NASA Apollo Body With the Use of Telemetry Data From Free-flight Range Testing*; ARL-TR-4271; U.S. Army Research Laboratory: Aberdeen Proving Ground, MD, September 2007.
15. Decker, R.; Kolsch, M.; Yakimenko, O. *A Computer Vision Approach to Automatically Measure the Spin-rate of Artillery Projectiles Painted with Stripes*. Naval Postgraduate School, Monterey, CA, December 2012.
16. Decker, R.; Kolsch, M.; Yakimenko, O. *A Computer Vision Approach to Automatically Measure the Spin-rate of Fin-Stabilized Projectiles Painted with Stripes*. Naval Postgraduate School, Monterey, CA, February 2013.
17. Clay, W. *A Precision Yawsonde Calibration Technique*; BRL-MR-2263; U.S. Army Ballistic Research Laboratory: Aberdeen Proving Ground, MD, January 1973.
18. Mermagen, W.; Clay, W. *The Design of a Second Generation Yawsonde*; BRL-MR-2368, U.S. Army Ballistic Research Laboratory: Aberdeen Proving Ground, MD, April 1974.
19. Davis, B.; Hall, R.; Harkins, T.; Wilson, M.; Patton, B.; Nair, M.; Ilg, M. *Integral Telemetry Module Development and Demonstration on the Precision-Guided Mortar Munition*; ARL-TR-4141; U.S. Army Research Laboratory: Aberdeen Proving Ground, MD, June 2007.
20. Lovas, A.; Brown, T.; Harkins, T. Innovative Technologies and Techniques for In-Situ Test and Evaluation of Small Caliber Munitions. *2007 Annual ITEA International Symposium*, Lihue, HI, October 2007.
21. Thompson, A. System and Method for Obtaining Attitude from Known Sources of Energy and Angle Measurements. U.S. Patent #7388538B1, June 2008.
22. Hepner, D.; Harkins, T. *Determining Inertial Orientation of a Spinning Body with Body-Fixed Sensors*; ARL-TR-2313; U.S. Army Research Laboratory: Aberdeen Proving Ground, MD, January 2001.
23. Harkins, T. *Understanding Body-Fixed Sensor Output from Projectile Flight Experiments*; ARL-TR-3029; U.S. Army Research Laboratory: Aberdeen Proving Ground, MD, September 2003.

INTENTIONALLY LEFT BLANK.

---

## Appendix A. The Aeroballistic Diagnostic Fuze (DFuze)

---

Ballistics engineers have long been using onboard sensor packages tied to telemetry (TM) transmitters or data recorders for measuring projectile motion and trajectory heading histories. This has proven to be a reliable means of gathering high-fidelity measurements during flight experiments of both developmental and inventory projectiles. The U.S. Army Research Laboratory (ARL) and its predecessor, the U.S. Ballistic Research Laboratory (BRL), have developed and employed custom TM systems to obtain data from onboard sensors for the measurement of in-flight projectile states for over 35 years. The first such system, a yawsonde, employed optical detectors on a rotating projectile. The TM system transmitted the detector's outputs, which were recorded and used to identify the times at which the sun was within the detector's field-of-view. Although not the first to use solar sensors, Clay (17) and Clay and Mermagen (18) were responsible for advancements that made yawsondes into precision angular measurement systems.

Mechanical devices, inertial sensors, and other types of transducers have long been available, but using this class of devices on board gun-launched ordnance projectiles was not generally practicable until the last few decades. Hardware meeting the criteria of size, weight, cost, performance, and survivability in the harsh projectile launch and flight environment were not then available. With the microelectronics revolution, the commercial sector began producing smaller and more capable components for industrial and consumer use. ARL is at the forefront of efforts to incorporate newly available off-the-shelf components for obtaining onboard projectile state measurements. For example, small and rugged accelerometers used for airbag deployment in automobiles are also usable for projectile acceleration measurements.

The Aeroballistic Diagnostic Fuze (DFuze) is a patented instrumentation system (2002) developed by personnel of the Guidance Technologies Branch of ARL. DFuze is a technological advancement of the yawsonde, packaged in a NATO-compatible artillery fuze shape. It contains high-g qualified miniature sensors, microelectronics, onboard data acquisition, a power supply, and the TM components necessary to obtain and transmit the desired measurements. The standard DFuze model circa 2003 sensor suite included three orthogonal axes of translational accelerometers, three orthogonal axes of vector magnetometers, three orthogonal axes of angular rate sensors, a yawsonde using four optical sensors, a constellation of four accelerometers configured and combined to yield a centripetal acceleration measurement, and a temperature sensor.

Custom designs employing these and other components are routinely made at ARL to instrument all manner of projectiles with systems packaged in different shapes, installed at different locations, equipped with different sensors, etc., to satisfy particular requirements and to meet particular experiment objectives.

Figure A-1 shows: (a) the standard DFuze; (b) a custom TM system integrated into the midbody of a mortar munition; (c) a custom TM system integrated into a subscale NASA Crew Exploration Vehicle; and (d) an onboard recorder system for a small-caliber projectile. These four systems are further described by Davis et al. (5), Davis et al. (19), Topper et al. (14), and Lovas et al. (20).

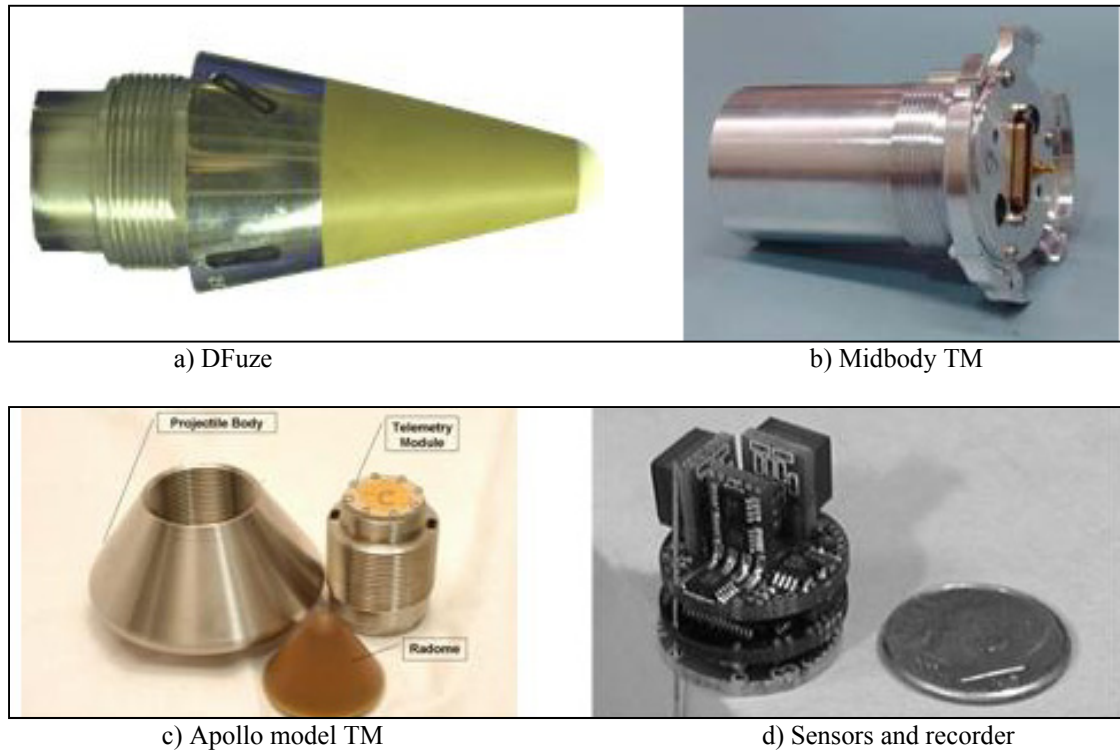


Figure A-1. Projectile state measurement systems.

Figure A-2 shows a standard DFuze installed on an artillery projectile. In instrumented flight experiments for a number of different inventory and developmental tank and artillery projectiles, the DFuze replaces the conventional tactical fuze while maintaining the projectile's mass and moment characteristics and external shape. This enables accurate aeroballistic characterization of the subject projectiles in their tactical configurations.



Figure A-2. DFuze instrumentation on the front of an artillery round.

Most recently, continuing advances to sensors and electronics, as well as specific customer requirements have led to several further instrumentation system variants at ARL. The Multifunctional Instrumentation and Data Acquisition System (MIDAS) and the Reusable

Instrumented Test Article (RITA) are some of more recent systems that, as their names imply, provide additional onboard sensing and processing capabilities and increased survivability, respectively. Global Positioning System (GPS) receivers are also sometimes included onboard gun- and tube-launched projectiles with their output included in the TM stream.

Generally, TM data are recorded at the test site and later processed to obtain time histories of the projectile states observable by the respective sensors. Projectile heading and roll rate with respect to the sun are obtained from yawsonde data. Projectile heading and roll rate with respect to the geomagnetic field are obtained from magnetometer data. Translational accelerations at various points in the projectile in desired directions are obtained from multiple accelerometers. Rotation rates about the sensor axis are obtained from each rate sensor. Pressures at particular locations on a flight body are obtained from pressure transducers. Temperature within the body is obtained from temperature transducers. Roll orientation is obtained from thermopile output proportional to the radiometric temperature within the sensor field-of-view. The GPS provides projectile position and velocity. Thompson at ARL has devised a method for obtaining heading of GPS-equipped spinning projectiles (21), which may be implemented in the future.

INTENTIONALLY LEFT BLANK.

---

## Appendix B. Projectile Orientation In Navigation TERms (POINTER)

---

More than 30 years of sensor development and field experiment experience at ARL have resulted in a capability of measuring solar-aspect angles and solar-plane crossing rates to subdegree and degree-per-second accuracies, respectively. Beginning in the 1990s, developments in magnetic sensing devices have enabled similar measurements to be made with respect to the earth's magnetic field. Data from a triaxial vector magnetometer can provide magnetic aspect angles and magnetic roll rates at the sensor sampling rates. With knowledge of the sun's position and magnetic field orientation, the combination of solar and magnetic sensors provides measurements from which the pitch, yaw, and roll angle history can be derived. This methodology, termed the Projectile Orientation In Navigation TERms (POINTER), has been successfully employed on telemetered data from numerous projectiles in flight experiments conducted on inventory and developmental projectiles (22).

The mathematical solution for projectile heading will first be described as a generalized system of simultaneous equations (section B-1). Next, the specific formulation employed with solar and magnetic data will be derived (section B-2). Finally, geometric issues regarding the accuracy of POINTER will be discussed (section B-3).

### B-1 Solving for Projectile Heading - Generalized Solution

The center of motion and the principal axis of rotation, i.e., the spin axis, of a 3-D free-flying solid body are described within a Cartesian coordinate system by three variables denoting location and two variables defining angular orientation. The derivative of the location with respect to time is commonly referred to as the velocity vector,  $\vec{V}$ . The principal axis of rotation of a spinning body is often not collinear with the velocity vector. In such cases, an orientation time history estimated from derivatives of location variables does not provide an accurate measure of the navigation pointing angles of the flight body. For a symmetric, spinning body, the navigation pointing vector,  $\vec{P}$ , is coincidental with the principal axis of rotation. The rotation rate of the body about this axis is commonly called the "spin rate." The Eulerian heading variables psi ( $\varphi$ ) and theta ( $\theta$ ) are used to denote the two angular components of azimuth and elevation required to orient the body principal axis of rotation within a right-handed navigation system. With the combination of body-fixed sensors measurements of the included angles between the axis of rotation and two distinct earth-fixed fields and knowledge of these fields' orientations in the navigation coordinate system,  $\varphi$  and  $\theta$  can be determined. Thus, a tabular pointing angle time history can be generated.

The generalized field transformation can be exemplified if we combine the coordinate system with two representative field vectors of known orientation,  $\vec{F}_1$ , and  $\vec{F}_2$ , to yield the angle definitions shown in figure B-1.

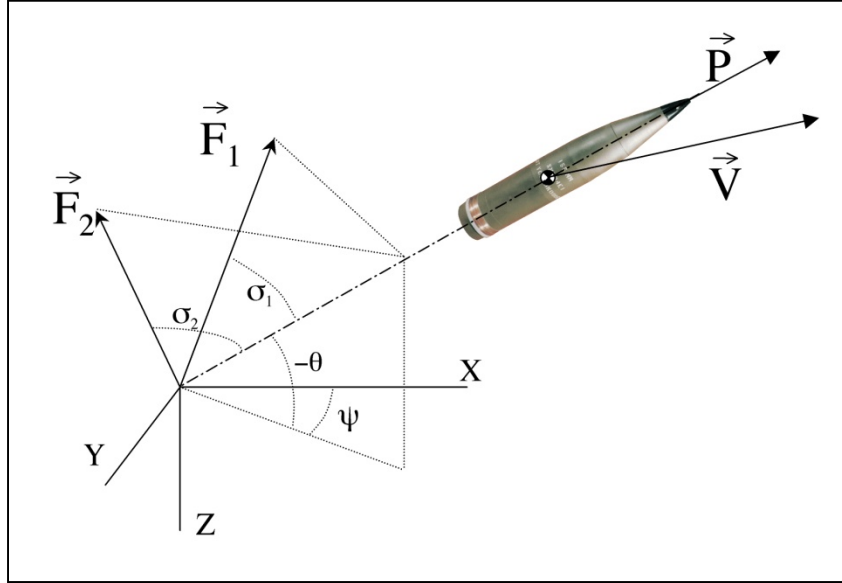


Figure B-1. A spinning body within a convenient navigation coordinate system.

Let the unit vectors  $\vec{P}$ ,  $\vec{F}_1$ , and  $\vec{F}_2$  along  $\vec{P}$ ,  $\vec{F}_1$ , and  $\vec{F}_2$  be defined within the navigation (X, Y, Z) system as:

$$\begin{aligned}\vec{P} &= (P_x, P_y, P_z) \\ \vec{F}_1 &= (F_{1_x}, F_{1_y}, F_{1_z}) \\ \vec{F}_2 &= (F_{2_x}, F_{2_y}, F_{2_z})\end{aligned}\quad (B-1)$$

The components of  $\vec{P}$  are obtained from the simultaneous solution of the system:

$$\begin{aligned}\vec{P} \cdot \vec{F}_1 &= \cos(\sigma_1) \\ \vec{P} \cdot \vec{F}_2 &= \cos(\sigma_2), \\ |\vec{P}| &= 1\end{aligned}\quad (B-2)$$

in which the field vectors ( $\vec{F}_1$ ,  $\vec{F}_2$ ) and the included angles ( $\sigma_1$ ,  $\sigma_2$ ) between  $\vec{P}$  and the respective field vectors are known, estimated, or measured.

## B-2 Solving for Projectile Heading - Application to Solar and Magnetic Sensor Data

Angular navigation parameters are most often described in an earth-fixed Cartesian coordinate system. Given a convenient navigation coordinate system (e.g., north, east, vertical) and an

arbitrary location  $L = (L_n, L_e, L_v)$ , let the unit vector from  $L$  to the sun be  $\vec{S} = (S_n, S_e, S_v)$  and the unit vector through  $L$  along the magnetic field be  $\vec{M} = (M_n, M_e, M_v)$ . Unfortunately, the angular variables in the system of equation B-2 describing heading are nonseparable in this coordinate system. In order to obtain the projectile heading angles, the vector along the projectile axis must be derived in a computationally convenient coordinate system and then transformed into the navigation coordinate system.

Consider a Cartesian coordinate system (A,B,C) with its origin at  $L$ , its +B axis along the solar vector, its A axis so that the local magnetic vector is in the half-plane containing the B axis and the +A axis, and its +C axis pointing in the direction that a right-hand threaded screw advances when its head is rotated from +A to +B (see figure B-2). This system will be referred to as the “solar” system.

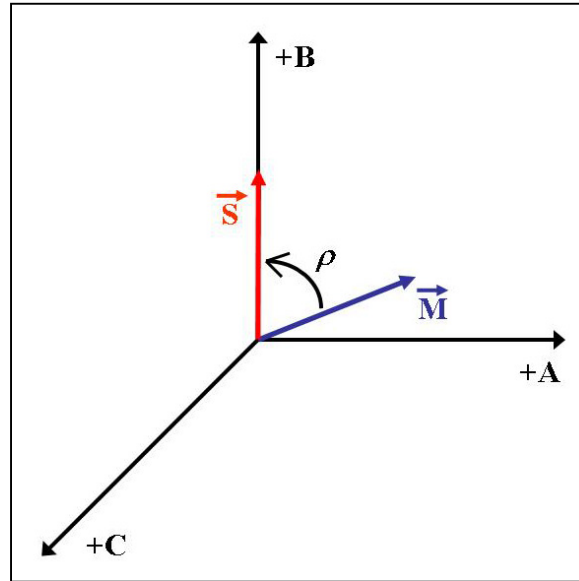


Figure B-2. The “solar” coordinate system.

Designating the angle between  $\vec{S}$  and  $\vec{M}$  as  $\rho$ , the mappings of the axes of the solar system to the navigation system are given by:

$$(0,1,0)_S \rightarrow (S_n, S_e, S_v) , \quad (B-3)$$

$$(0,0,1)_S \rightarrow (\vec{M} \times \vec{S}) / \sin \rho , \quad (B-4)$$

$$(1,0,0)_S \rightarrow \vec{S} \times [(\vec{M} \times \vec{S}) / \sin \rho] , \quad (B-5)$$

in which  $\rho = \cos^{-1}(\vec{S} \bullet \vec{M})$ . Evaluating the cross-products in equations B-4 and B-5 yields expressions for the components of the respective mappings:

$$\vec{M} \times \vec{S} = (M_e S_v - M_v S_e, M_v S_n - M_n S_v, M_n S_e - M_e S_n) , \quad (B-6)$$

$$\therefore (0,0,1)_S \rightarrow (M_e S_v - M_v S_e, M_v S_n - M_n S_v, M_n S_e - M_e S_n) / \sin \rho, \quad (\text{B-7})$$

$$\begin{aligned} \vec{S} \times (\vec{M} \times \vec{S}) &= \vec{S} \times (M_e S_v - M_v S_e, M_v S_n - M_n S_v, M_n S_e - M_e S_n) \\ &= \begin{pmatrix} S_e (M_n S_e - M_e S_n) - S_v (M_v S_n - M_n S_v), \\ S_v (M_e S_v - M_v S_e) - S_n (M_n S_e - M_e S_n), \\ S_n (M_v S_n - M_n S_v) - S_e (M_e S_v - M_v S_e) \end{pmatrix}, \end{aligned} \quad (\text{B-8})$$

$$\therefore (1,0,0)_S \rightarrow \begin{pmatrix} M_n (S_e^2 + S_v^2) - S_n S_e M_e - S_n S_v M_v, \\ M_e (S_n^2 + S_v^2) - S_n S_e M_n - S_e S_v M_v, \\ M_v (S_n^2 + S_e^2) - S_n S_v M_n - S_e S_v M_e \end{pmatrix} / \sin \rho. \quad (\text{B-9})$$

Any vector defined in the ‘‘solar’’ system,  $\vec{V}_S = (v_A, v_B, v_C)$ , can be transformed to its representation in the navigation system,  $\vec{V}_N = (v_n, v_e, v_v)$ , by

$$\vec{V}_N = \begin{pmatrix} t_{1,1} & t_{1,2} & t_{1,3} \\ t_{2,1} & t_{2,2} & t_{2,3} \\ t_{3,1} & t_{3,2} & t_{3,3} \end{pmatrix} \vec{V}_S, \quad (\text{B-10})$$

where,

$$\begin{aligned} t_{1,1} &= (M_n (S_e^2 + S_v^2) - S_n S_e M_e - S_n S_v M_v) / \sin \rho \\ t_{1,2} &= (M_e (S_n^2 + S_v^2) - S_n S_e M_n - S_e S_v M_v) / \sin \rho \\ t_{1,3} &= (M_v (S_n^2 + S_e^2) - S_n S_v M_n - S_e S_v M_e) / \sin \rho \\ t_{2,1} &= S_n \\ t_{2,2} &= S_e \\ t_{2,3} &= S_v \\ t_{3,1} &= (M_e S_v - M_v S_e) / \sin \rho \\ t_{3,2} &= (M_v S_n - M_n S_v) / \sin \rho \\ t_{3,3} &= (M_n S_e - M_e S_n) / \sin \rho \end{aligned} \quad (\text{B-11})$$

Given solar aspect angle ( $\sigma_S$ ) and magnetic aspect angle ( $\sigma_M$ ) histories derived from solarsonde and magsonde reductions (23), these data should be interpolated onto a common time base. Then, at every time step, the components of a unit vector ( $\vec{P}$ ) along the projectile spin axis can be readily determined in the solar system (see figure B-3).

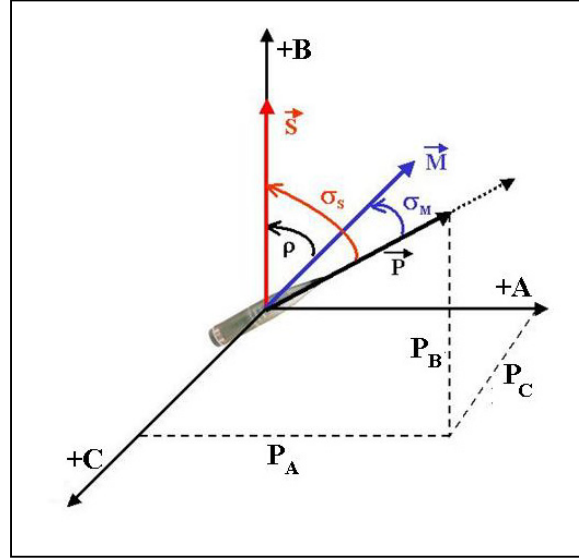


Figure B-3. Components of the projectile pointing vector in the “solar” system.

$$\cos \sigma_S = (0, 1, 0) \cdot (P_A, P_B, P_C) = P_B, \quad (\text{B-12})$$

$$\cos \sigma_M = (\sin \rho, \cos \rho, 0) \cdot (P_A, P_B, P_C) = P_A \sin \rho + P_B \cos \rho, \quad (\text{B-13})$$

by substitution,

$$P_A = \frac{\cos \sigma_M - \cos \sigma_S \cos \rho}{\sin \rho}, \quad (\text{B-14})$$

$$\begin{aligned} P_C &= \pm \sqrt{1 - P_A^2 - P_B^2} \\ &= \pm \sqrt{1 - \cos^2 \sigma_S - \left( \frac{\cos \sigma_M - \cos \sigma_S \cos \rho}{\sin \rho} \right)^2}, \end{aligned} \quad (\text{B-15})$$

or

$$P_C = \pm \sqrt{\sin^2 \sigma_S - \left( \frac{\cos^2 \sigma_M - 2 \cos \sigma_M \cos \sigma_S \cos \rho + \cos^2 \sigma_S \cos^2 \rho}{\sin^2 \rho} \right)}. \quad (\text{B-16})$$

The sign ambiguity of  $P_C$  is usually easily resolved with knowledge of the initial navigation orientation (e.g., launcher orientation).

Finally, per equation B-10, the components in the navigation system of a unit vector along the projectile axis of rotation are given by:

$$(P_n, P_e, P_v) = \begin{pmatrix} t_{1,1} & t_{1,2} & t_{1,3} \\ t_{2,1} & t_{2,2} & t_{2,3} \\ t_{3,1} & t_{3,2} & t_{3,3} \end{pmatrix} (P_A, P_B, P_C), \quad (\text{B-17})$$

and the corresponding heading angles by,

$$\theta = \tan^{-1} \left( \frac{P_v}{\sqrt{(P_n^2 + P_e^2)}} \right) \quad \text{where} \quad -\pi/2 \leq \theta \leq \pi/2, \quad (\text{B-18})$$

$$\psi = \tan^{-1}(P_e/P_n) \quad \text{where} \quad -\pi \leq \psi \leq \pi. \quad (\text{B-19})$$

### B-3 Effect of Measurement Geometry on Accuracy of POINTER

Because of the nonlinearity of the trigonometric functions in the governing equations, POINTER heading estimates can be extremely sensitive to errors in the estimates of the inertial orientation of the solar field vector and the local magnetic field vector, and to errors in the estimates of the included angles between the projectile axis and the respective field vectors. The ideal geometry both for computational accuracy and for sensor measurements of the included angles would have the vector from the projectile to the sun, the geofield vector at the projectile location, and the projectile velocity vector form an orthogonal triad. For the spatial extent and temporal duration of most ballistic projectile trajectories, there are little or no changes in relative orientations of the solar and magnetic vectors, but the inertial heading of the velocity vector obviously changes as the projectile progresses along its trajectory—so the included angles between the velocity vector and the sun and geofield are also changing. As the geofield vector changes with location, altitude, and date; the solar vector changes with location, date, and time of day; and the gun shotline can change with test site; available options can be analyzed to design a test plan that achieves the best possible measurement conditions within the available design space.

The flight experiments covered in this report were conducted on October 18, 2012 at a gun position at Yuma Proving Grounds (YPG) located at 32.87° north latitude and 114.43° west latitude. The geofield vector components at that site were 58.61° inclination (down from horizontal) and 11.39° declination (east of true north). As the sun traverses its arc throughout the day, the included angle between the vector from the projectile to the sun and the geofield vector constantly changes. This changing measurement geometry is seen in figure B-4. If the solar vector and geofield vector are parallel or antiparallel, the projectile solar aspect angle measurement and magnetic aspect angle measurement are completely redundant and equation B-2 becomes an underdetermined system. Though equation B-2 is theoretically solvable for all other conditions (i.e., with perfect knowledge of  $\bar{F}_1, \bar{F}_2, \sigma_1, \sigma_2$ ), a useful rule of thumb for

achieving reliable heading estimation with experimentally derived data is that the solar and geofield vectors be within  $60^\circ$  of perpendicular. Between 11:00 a.m. and approximately 2:30 p.m. this condition was not satisfied.

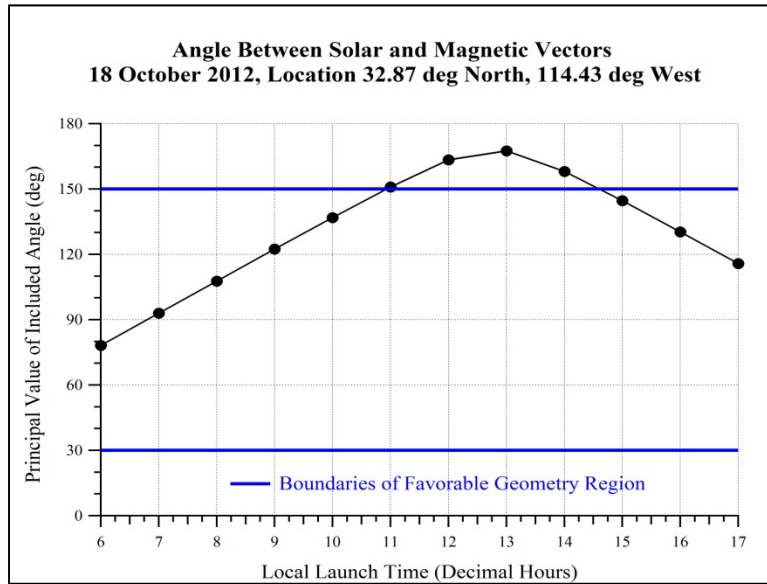


Figure B-4. Relative orientation of solar and magnetic vectors at experiment site.

A similar metric is applied to the heading of the projectile with respect to the plane defined by the two unit field vectors, i.e.,  $\vec{F}_1, \vec{F}_2$ . In this case, the issue is choosing the correct root of equation B-16. For most ballistic trajectories, the azimuthal component of the projectile heading never differs very much from the azimuth of the launcher line of fire. The shotline for these experiments was  $84^\circ$  east of north. The family of curves in figure B-5 gives the angle between the solar/magnetic plane and possible headings along that shotline at the same times as shown in figure B-4. We designate this angle as  $\varepsilon$ . The greater the magnitude of this out-of-plane angle for an anticipated trajectory, the less likely that the actual projectile heading will result in equation B-16 ambiguity. In postprocessing, an experienced analyst can usually resolve any such ambiguity—but this can be time consuming and tedious.

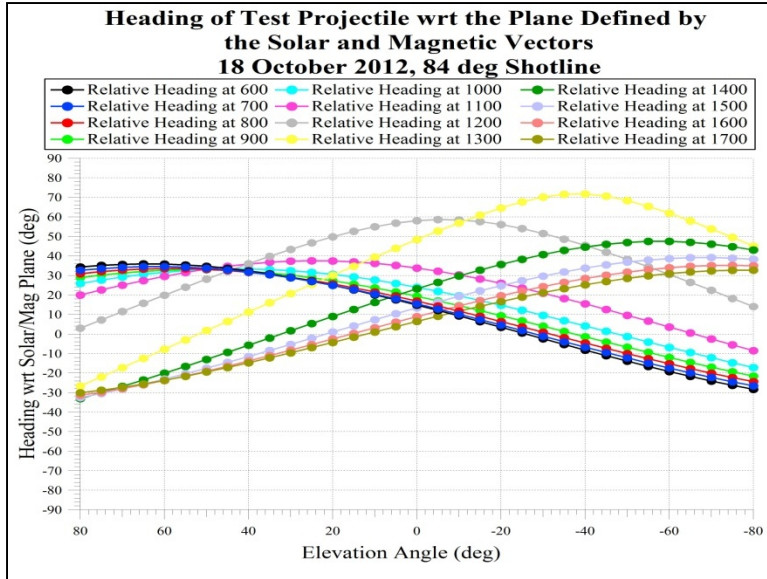


Figure B-5. Angle between projectile heading and plane containing solar and magnetic vectors.

A numerical scoring metric reflecting the influence of both of the preceding angular relationships was devised to provide a convenient and useful tool for assessing the suitability of flight experiment geometries for POINTER processing. This tool can be used as an aid for designing experiments to provide the best possible conditions for POINTER analysis. Scores range from 0 (unacceptable) to 1 (best) and are computed as  $S = 0$  if  $|90 - \rho| < 60$  or  $|\varepsilon| < 10$ . Otherwise,  $S = \sin(\rho) * \sin(\varepsilon)$ . In figure B-6, the scores metric is shown for the date, location, and shotline of the flight experiments in this report. Each of the curves gives the score versus projectile elevation angle at the time of day contained in the curve name. Because the plot ordinate range is from 0.1 to 1.0, curves or portions of curves that are unacceptable are not displayed, e.g., 11:00 → 14:00. The gun QE was  $28.1^\circ$  for both of the flight experiments and the respective launch times were 9:36 a.m. and 10:31 a.m. It is seen in figure B-6 that the experiment geometry was acceptable for POINTER estimation of projectile early flight angular motion (where the projectile elevation angle would be close to the QE) only for experiments conducted before 11 a.m.

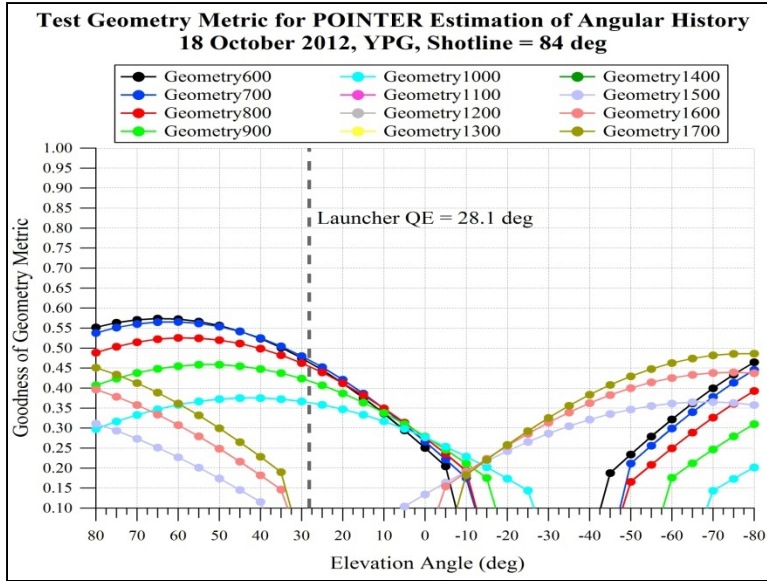
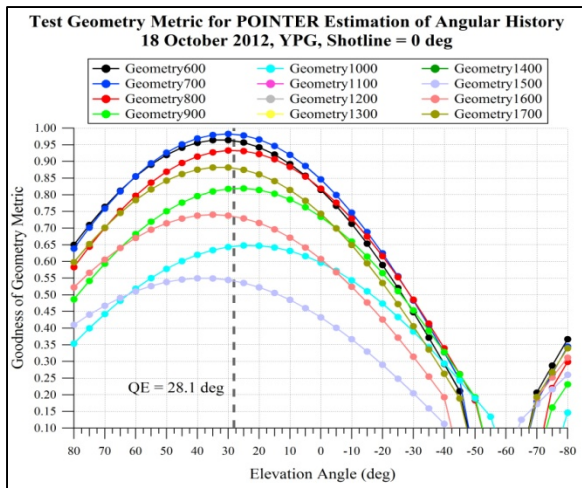
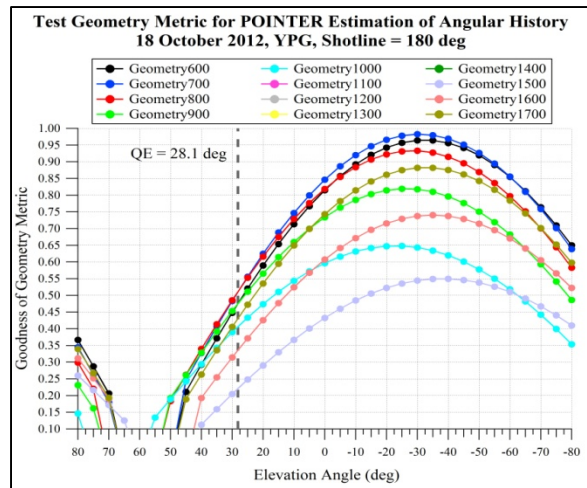


Figure B-6. POINTER suitability scoring at YPG experiment site.

Test engineers can use this tool when planning flight experiments for which POINTER analysis is desired to inform choices among available options. Figure B-7 gives examples of the scoring variations with shotline. Figure B-8 gives examples of the scoring variations with date. Figure B-9 gives examples of the scoring variations with location.

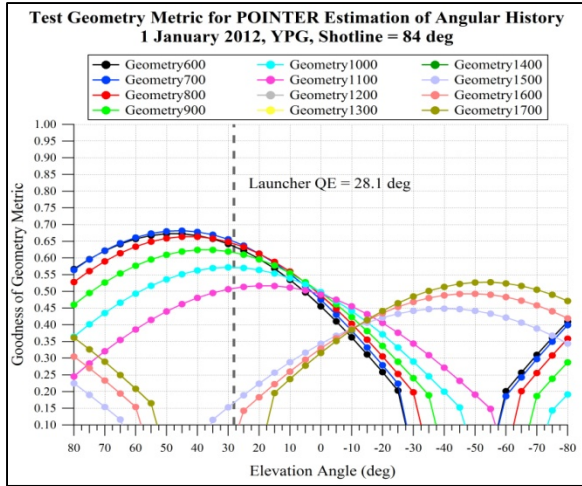


a) YPG, 18 October 2012, Shotline=0°

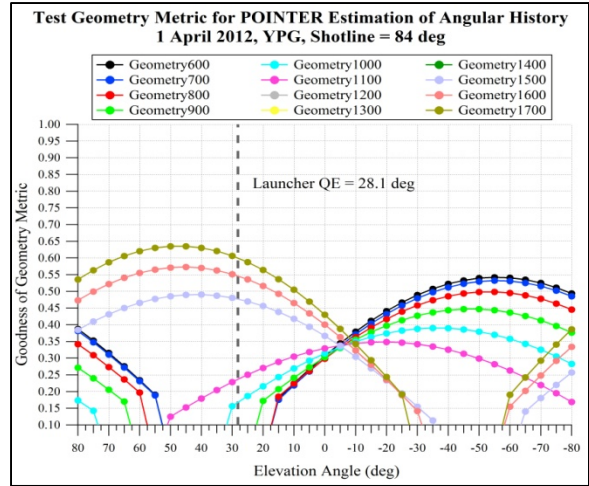


b) YPG, 18 October 2012, Shotline=180°

Figure B-7. POINTER suitability scoring at YPG experiment site for two shotlines.

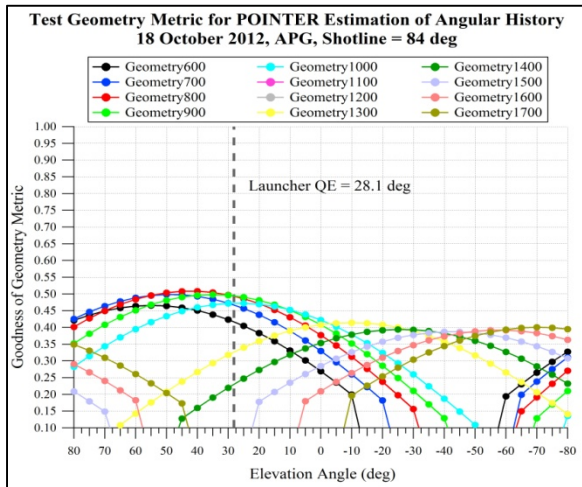


a) YPG, 1 January 2012, Shotline=84°

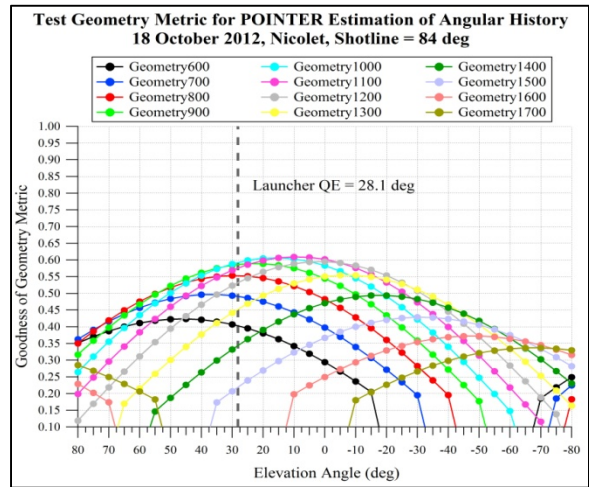


b) YPG, 1 July 2012, Shotline=84°

Figure B-8. POINTER suitability scoring at YPG experiment site for two test dates.



a) APG, 18 October 2012, Shotline=84°



b) Nicolet, 18 October 2012, Shotline=84°

Figure B-9. POINTER suitability scoring at two experiment sites.

---

## List of Symbols, Abbreviations, and Acronyms

---

ARDEC	U.S. Armaments Research and Development Center
ARL	U.S. Army Research Laboratory
BRL	U.S. Ballistic Research Laboratory
DFuze	Diagnostic Fuze
GPS	Global Positioning System
IRIG	International Range Instrumentation Group
MIDAS	Multifunctional Instrumentation and Data Acquisition System
NPS	Naval Postgraduate School
POINTER	Projectile Orientation In Navigation TERms
QE	quadrant elevation
RITA	Reusable Instrumented Test Article
TM	telemetry
YPG	Yuma Proving Grounds

NO. OF  
COPIES ORGANIZATION

1 DEFENSE TECHNICAL  
(PDF) INFORMATION CTR  
DTIC OCA

1 DIRECTOR  
(PDF) US ARMY RESEARCH LAB  
IMAL HRA

1 DIRECTOR  
(PDF) US ARMY RESEARCH LAB  
RDRL CIO LL

1 GOVT PRINTG OFC  
(PDF) A MALHOTRA

ABERDEEN PROVING GROUND

2 USARL  
(PDF) RDRL WML F  
B DAVIS  
T HARKINS